NACA

RESEARCH MEMORANDUM

EXPERIMENTAL INVESTIGATION OF A TRANSONIC AXIAL-FLOW-COMPRESSOR ROTOR WITH DOUBLE-CIRCULAR-ARC AIRFOIL BLADE SECTIONS

I - DESIGN, OVER-ALL PERFORMANCE AND STALL CHARACTERISTICS

By George W. Lewis, Jr., Francis C. Schwenk
and George K. Serovy

Lewis Flight Propulsion Laboratory
Cleveland, Ohio

NATIONAL ADVISORY COMMITTEE
FOR AERONAUTICS

WASHINGTON

April 5, 1954

Classification cancelled (or changed to UNCLASSIFIED)

By Authority of NBA Tech Pub Amendment No 2
(OFFICER AUTHORIZED TO CHANGE)

By W Dodd
NAME AND

GRADE OF OFFICER MAKING CHANGE)

1 Mar 61
DATE

NATIONAL ADVISORY COMMITTEE FOR AERONAUTICS

RESEARCH MEMORANDUM

EXPERIMENTAL INVESTIGATION OF A TRANSONIC AXIAL-FLOW-COMPRESSOR ROTOR WITH DOUBLE-CIRCULAR-ARC AIRFOIL BLADE SECTIONS

I - DESIGN, OVER-ALL PERFORMANCE, AND STALL CHARACTERISTICS

By George W. Lewis, Jr., Francis C. Schwenk, and George K. Serovy

SUMMARY

An experimental transonic axial-flow-compressor rotor was designed, constructed, and tested to supply experimental blade-element data for double-circular-arc airfoil sections. The rotor was designed to operate at a corrected tip speed of 1000 feet per second, to obtain an average total-pressure ratio of 1.34, and to pass a corrected specific weight flow of 30.7 pounds per second per square foot of frontal area. The hub-tip radius ratio at the rotor inlet was 0.50. This report presents the rotor design method, over-all performance based on fixed-rake measurements, and stall characteristics.

At design corrected tip speed, a peak rotor efficiency of 89 percent was obtained at a corrected specific weight flow of 30.5 pounds per second per square foot with an average rotor total-pressure ratio of 1.41. At speeds less than design, the peak rotor efficiency was about 92 percent; whereas, the peak efficiency for 106.4-percent design speed was about 87 percent.

Rotating-stall and surge characteristics were observed in detail at 60 percent of design speed for both decreasing and increasing weight flows. For this compressor rotor, rotating-stall zones (2 and 3 in number) and a surge condition were noted.

INTRODUCTION

It has been shown in references 1 and 2 that the transonic axial-flow-compressor inlet stage is capable of operation at high weight flows per unit frontal area and high levels of pressure ratio with no sacrifice in efficiency over conventional subsonic-compressor stages. The transonic compressor of references 1 and 3 used an airfoil shape at the rotor tip (high Mach number region) that approximated a double-circular-arc section but differed somewhat in mean-line shape and thickness distribution. Another inlet-stage rotor (ref. 2) designed with double-circular-arc airfoils also showed good performance in the transonic region (i.e.,

for Mach numbers up to 1.2). Since the available experimental data seem to indicate that the double-circular-arc airfoil can be used in transonic compressors (up to Mach numbers of 1.2) with resulting high efficiencies, the double-circular-arc airfoil has been chosen as a basic type in order to simplify the problems of compressor design. A recent analytical investigation reported in reference 4 showed that compressor airfoils designed to produce a desirable chordwise velocity (or loading) distribution are similar to double-circular arcs for Mach numbers between 0.8 and 1.2.

The problem of compressor design can be considered to consist of two phases: (1) the computation of the radial distribution of flow properties entering and leaving each blade row and (2) the selection of the proper blade row that will produce the desired flow conditions. The radial variation of the flow properties at the outlet of a compressor blade row can be computed by means of the radial-equilibrium concept, which includes the effects of radial variation of losses (refs. 2 and 3). Consequently, good design control will depend to some extent on a knowledge of the loss variation at the outlet of the blade rows.

The complete blade row can then be constructed by radially stacking blade sections selected to produce the desired outlet conditions. This selection can be made on the basis of blade-element performance of the airfoil sections to be used. Reference 5 gives a discussion of the necessary blade-element performance parameters and discusses the importance of having accurate information in order to design high-performance compressor rotors. Unfortunately, little blade-element data for the double-circular-arc airfoil is yet available for the required range of solidities, stagger angles, and cambers. Reference 3 presents methods and significant parameters for determining cascade-type blade-element data from rotor tests; and, in view of the critical nature of the design of transonic compressors, it is desirable to obtain the double-circular-arc blade-element data in this manner.

The rotor described in this report was designed with double-circular-arc airfoil sections and, as such, represents part of a test program initated at the NACA Lewis laboratory to provide blade-element data for double-circular-arc airfoil sections that will be applicable to the design of transonic axial-flow-compressor stages. Comparisons between the measured rotor-outlet conditions and those computed from the radial-equilibrium equation will give a further insight into the problem of computing rotor-outlet conditions in the design case.

The compressor rotor under consideration was designed for a total-pressure ratio of 1.34 at a corrected rotor tip speed of 1000 feet per second with a rotor-inlet hub-tip radius ratio of 0.50. The design relative rotor-inlet Mach numbers ranged between 0.76 at the hub and 1.10 at the tip. The design corrected specific weight flow was 30.7 pounds per second per square foot of frontal area.

This preliminary report provides additional over-all performance characteristics of transonic axial-flow-compressor inlet stages. Included are the design procedure, the over-all performance of the rotor operating at 60, 80, 90, 100, and 106.4 percent of design speed, and rotating-stall data.

SYMBOLS

The following symbols are used in this report. A diagram illustrating the air and blade angles and the velocities is presented in figure 1 to define some of the symbols more completely.

A_f compressor frontal area based on rotor tip diameter, sq ft

D diffusion factor, $D = 1 - \frac{V'_4}{V'_3} + \frac{V'_{\theta,3} - V'_{\theta,4}}{2\sigma V'_3}$ (ref. 6)

i incidence angle, angle between inlet relative air-velocity vector and tangent to blade mean line at leading edge, deg

M Mach number

N rotational speed of rotor, rps

P total pressure, lb/sq ft

r radius measured from axis of rotation, in.

U blade speed, ft/sec

V air velocity, ft/sec

W air weight flow, lb/sec

β air-flow angle measured from axis of rotation, deg

γ ratio of specific heats, 1.40

γ° blade angle, direction of tangent to blade mean camber line at leading or trailing edge measured from axis of rotation, deg

δ ratio of inlet total pressure to NACA standard total pressure, $P_1/2117$

δ° deviation angle, angle between outlet relative air-velocity vector and tangent to blade mean line at trailing edge, deg

η adiabatic temperature-rise efficiency

θ ratio of inlet total temperature to NACA standard temperature, $T_1/518.6$

σ solidity, ratio of blade chord measured along streamline to average blade spacing

Subscripts:

m mean radius

t tip of rotor

z axial direction

θ tangential direction

1 depression tank

2 upstream of rotor, location of inlet static-pressure rake

3 rotor inlet

4 rotor-outlet survey station

5 stator outlet

6 compressor outlet, discharge measuring station

Superscript:

' denotes conditions relative to a blade row

COMPRESSOR DESIGN

Velocity-Diagram Calculations

In the design of this transonic axial-flow-compressor rotor, no attempt was made to maximize the values of total-pressure ratio or corrected specific weight flow, since this test program was initiated to determine the blade-element performance for a compressor operating in a range currently of interest. Although only the rotor was constructed and tested, the design calculations were conducted for a complete transonic-compressor inlet stage (including rotor and stator blade rows) from which the air discharges axially.

A 14-inch tip diameter is used in this design. The design corrected rotor tip speed was selected in the range of values used for conventional multistage axial-flow compressors and was set at 1000 feet per second. No inlet guide vanes were used; and a conventional value of 0.60 was chosen for the inlet absolute Mach number, which produces a corrected weight flow per square foot of frontal area of 30.7 pounds per second for an inlet hub-tip radius ratio of 0.50 and an assumed radially constant inlet absolute Mach number. A blockage factor (ratio of actual weight flow to ideal weight flow) of 0.985 was assumed at the rotor inlet to account for the annulus area reduction caused by both the inner and outer wall boundary layers. The resulting rotor-inlet relative Mach number was 1.10 at the tip, which is within the range of Mach numbers for which experience shows no resulting sacrifice in efficiency level.

A radially constant work input was chosen, and the stage total-pressure ratio was set at 1.33, a value which would result in a low rotor tip diffusion factor D. This total-pressure-ratio level is somewhat lower than that reported for the transonic compressor of references 1 and 3, which produced a relatively large radial gradient in total energy at the rotor outlet. In general, a higher average total-pressure ratio can be obtained for a given tip diffusion factor by using a radially increasing work-input gradient instead of a constant energy addition.

As a result of the conservative nature of the design, a stage adiabatic efficiency of 0.90 and a rotor adiabatic efficiency of 0.93 were assumed. The efficiencies were considered radially constant; consequently, application of the simple-radial-equilibrium concept produced radially constant axial velocities at the rotor- and stator-outlet stations. The computed rotor total-pressure ratio was 1.34.

Finally, the design was completed with the establishment of the hub contour. The stator-outlet hub radius was computed to satisfy continuity of weight flow by assuming a stator-outlet velocity of 650 feet per second (axial in direction) and a wall boundary-layer blockage factor of 0.94. The hub radius at the rotor outlet was determined by fairing a smooth curve between the inlet hub and the stator-outlet station as shown in figure 2. This procedure required an estimation of the axial chords of both rotor and stator blade rows and the spacing between the rows. Rotor-outlet conditions were then computed with a wall boundary-layer blockage factor of 0.95.

The rotor velocity diagrams were calculated for assumed streamlines that pass through equal-percentage radial increments of the passage height at each axial station. The design vector diagrams for the tip, mean, and hub streamlines are given in figure 3.

Blade Selection

The complete rotor blade row was designed by selecting double-circular-arc airfoil sections to produce the design flow conditions along the assumed streamlines on the basis of data on incidence angle i and deviation angle δ° in reference 3. The design incidence angles i varied linearly from 3° at the tip to 4° at the hub. Values for deviation angles δ° were set at 8° at the tip and 10° at the hub. A subsequent check revealed that these values assumed for deviation angles are too high. [Carter's rule (ref. 7) indicates that better values for deviation angle would be 3° at the tip and 6° at the hub of the rotor.] More recent considerations of design deviation angles for circular-arc airfoils are given in reference 5.

A solidity σ of 1.0 was selected for the tip of the rotor, and 19 blades were then required for a 14-inch-tip-diameter rotor to give a tip chord length of 2.32 inches. The solidity σ at the hub of the rotor was set at approximately 1.70, which requires a chord length of 2.09 inches. The chord length was varied uniformly along the span.

The maximum thickness of the tip airfoil section was 5 percent of the chord; and thickness was increased hyperbolically along the blade to an 8-percent maximum thickness for the hub airfoil section. Channel flow calculations for a stream filament along the hub indicated that a choking condition should not occur at the design point. Leading- and trailing-edge radii of 0.015 inch were used for all sections.

Table I shows the design and measured blade geometry for sections along assumed streamlines. It may be noted that some differences between the design and measured blade angles do exist. Figure 4 is a photograph of the 19-blade rotor.

APPARATUS AND PROCEDURE

Compressor Installation

The installation for this rotor test is described in reference 2. Power was supplied to the compressor by a 1500-horsepower dynamometer through a speed-increasing gearbox. Room air was drawn through a thin-plate sharp-edged orifice into an orifice tank and then passed into a depression tank and into the compressor through a bellmouth at the depression-tank exit (fig. 2). The air passed from the compressor into a collector and was discharged into the laboratory altitude exhaust system.

Instrumentation

Air flow through the compressor was measured by means of a sharp-edged thin-plate orifice. Pressure drop across the orifice was indicated on a micromanometer, and the orifice temperature was measured by four iron-constantan thermocouples.

The location of the instrumentation in the test rig is shown in figure 2. Station 1 is located in the depression tank. Stations 2 and 3 are 1.195 and 0.125 inches upstream of the rotor disk, respectively. Stations 4, 5, and 6 are located downstream of the rotor 0.50, 3.00, and 6.18 inches, respectively. At stations 2, 3, 4, 5, and 6, four static taps were located on both the outer and inner walls with approximately equal circumferential spacing.

Depression-tank (inlet) temperature measurements were made with 20 iron-constantan thermocouples, four each at area centers of five equal annular areas. Depression-tank total or stagnation pressure was obtained from five probes located at the same radii as the temperature probes.

A five-tube radial L static-pressure rake (fig. 5(a)) was installed upstream of the rotor at station 2 to determine the radial variation of static pressure. The tubes on the rake were spaced to divide the passage height into equal-percentage radial increments and were set parallel to assumed streamlines in the contracting inlet passage. The static-pressure readings were corrected for local Mach number effects. Total-pressure rakes (fig. 5(b)) were also located at station 2 to measure variations near the inner and outer walls.

Rotor-outlet conditions were determined from radial surveys of static pressure, total pressure, total temperature, and flow angle, taken 1/2 inch downstream of the rotor (station 4). The radial variation of rotor-outlet static pressure was sensed by an L-head Prandtl tube having two static-pressure orifices manifolded together (fig. 5(c)). Angle-sensing tubes were mounted on the L-head static tube to direct the probe into the flow. Static-pressure readings were corrected for local Mach number effects. Total-pressure, total-temperature, and flow-angle surveys were made with the combination claw, total-pressure, and total-temperature probe shown in figure 5(d). The two temperature readings taken on each combination probe were averaged at each radial position and corrected for local Mach number effects.

Outlet conditions for computing over-all rotor performance were determined from pressures and temperatures measured at station 6 by four radial shielded total-pressure rakes (fig. 5(e)) and four radial spike-type iron-constantan thermocouple rakes (fig. 5(f)) spaced equally around the

circumference of the casing. The five sensing elements on each of the rakes were located at centers of five equal annular areas. The temperature rakes were calibrated in an open jet calibration tunnel for angle and Mach number corrections. The temperature and pressure rakes were set at an average rotor-discharge angle for the range of conditions tested. The corrections due to pitch and yaw angles encountered in these tests were small; hence, no angle corrections were applied to the temperature readings.

The flow fluctuations of rotating stall were detected and measured with constant-temperature hot-wire anemometers. The anemometer probes were made with 0.0002-inch-diameter tungsten wire with an effective length of 0.08 inch. Observations were made with a dual-beam oscilloscope. The auxiliary equipment used is that discussed in reference 8.

Two hot-wire-anemometer probes were installed in radially transversing mechanisms about 1/2 inch downstream of the rotor (station 4, fig. 2). Four survey locations on the circumference were used to vary the angle between the two probes to permit the determination of the number of stall zones (ref. 9).

Over-All Performance Tests

The over-all performance of this rotor was obtained for a range of weight flows at each of the following corrected tip speeds: 600, 800, 900, 1000, and 1064 feet per second. The maximum weight flow at each speed was limited by a choking condition in the rotor or rig piping. The lowest weight flow tested at each speed was slightly greater than the weight flow at which it was impossible to read the pressures and temperatures because of unsteadiness of the readings.

The depression-tank pressure was maintained constant at 24 inches of mercury absolute by varying a butterfly control valve upstream of the inlet tank. The depression-tank temperature varied from 63° to 83° F, depending on the ambient conditions in the room. The blade-chord Reynolds number at design speed was approximately 920,000 for the tip of the rotor.

The data measured by the fixed rakes located at station 6 were numerically averaged in computing the average over-all performance.

Rotating-Stall Characteristics

After the over-all rotor performance data had been obtained, hot-wire anemometers were employed to investigate the stall patterns behind the rotor for 60-percent speed. This speed was selected because rotating-stall characteristics are most important at the lower speeds

for multistage-compressor applications. The stall patterns were observed or photograhed from a dual-beam cathode-ray oscilloscope for both increasing and decreasing weight flow. The number of rotating-stall regions was determined by employing the calculation procedure of reference 9.

RESULTS AND DISCUSSION

Over-All Performance

The average over-all performance of the transonic-compressor rotor as measured 6.18 inches downstream of rotor (station 6) is given in figure 6 as plots of adiabatic efficiency η and total-pressure ratio P_6/P_1 against corrected specific weight flow $W\sqrt{\theta}/\delta A_f$. At design speed (1000 ft/sec, fig. 6(d)), the measured peak over-all efficiency was 0.89 at a total-pressure ratio of 1.41 and a corrected specific weight flow of 30.5 pounds per second per square foot (very close to design value of 30.7). The efficiency level of this rotor as determined from a numerical average of the fixed-rake data is about 0.03 lower than the mass-averaged efficiency of the transonic rotor of reference 3. This difference is probably due primarily to the different averaging methods employed and not to any deficiency in the aerodynamic performance of the double-circular-arc blade elements. Unpublished results of a preliminary detailed survey indicate that the design-speed mass-averaged efficiencies will be higher than the values given on figure 6. At corrected tip speeds lower than design (figs. 6(a) to (c)), the peak efficiencies were between 0.92 and 0.93; however, the peak efficiency for the overspeed data (fig. 6(e)) decreased to a value of about 0.86. The rotor exhibited a wide, highly efficient weight-flow operating range at the lower speeds.

Rotor-Inlet Conditions

The computations of inlet conditions were made with the absolute inlet velocity considered axial in direction (no inlet guide vanes). The static-pressure variation along the radius at the rotor inlet (station 3) was faired between the outer and inner wall static-tap readings with a trend similar to that recorded from the inlet static-pressure rake (station 2). The procedure was justifiable, because there was only a small difference between the static pressures at stations 2 and 3.

Figure 7(a) shows the variation of measured inlet absolute Mach number with radius for a test point close to peak-efficiency operation at design speed. It can be seen that a radial variation of the inlet absolute Mach number did exist contrary to the design assumption of a constant value. The gradient was caused by the effects of the curvature of the inlet bellmouth.

The effect of the inlet gradient on the rotor-inlet relative Mach number is shown on figure 7(b), where the radial variation of design Mach

number is compared with the measured Mach number distribution for peak-efficiency operation at design speed. There is little difference between the two relative Mach numbers due to the difference between the design and measured rotor-inlet absolute Mach numbers.

In order to show a more important effect of the inlet absolute Mach number gradient, the design and experimental incidence angles are compared on figure 7(c). In this figure, the design incidence angles are based on the measured blade angles and are, therefore, not equivalent to the values given in the section on Blade Selection. Figure 7(c) shows that the difference between the actual and design inlet absolute Mach number variations caused a decrease in the incidence angle of 1.2° at the tip and an increase of 2.1° at the hub. Since the high Mach number blade-element performance characteristics are sensitive to incidence angle (refs. 3 and 5), it may be necessary to account for the presence of inlet absolute Mach number gradients when designing transonic compressors.

Rotor-Outlet Conditions

Rotor-outlet conditions, measured by survey instruments at station 4, are given on figure 8 as the radial variations of rotor total-pressure ratio P_4/P_1, rotor-outlet absolute air angle β_4, and rotor-outlet absolute Mach number M_4. The outlet conditions given in figure 8 were computed from data recorded near the peak-efficiency point of operation at design speed. The design conditions are also shown. The pressure-ratio curve indicates that the greatest departure from the design pressure-ratio level occurred near the rotor tip, where the measured rotor total-pressure ratio P_4/P_1 is 1.46. As indicated previously, the design values for deviation angle were chosen too high. Particularly at the rotor tip section, the effects of the resulting overturning of the air on the pressure ratio will be quite large because of the large blade-setting angles and the high blade speed. Reference 5 indicates the sensitivity of transonic-compressor performance to errors in deviation-angle selection.

Another consequence of the overturning was that the actual value for rotor tip diffusion factor D (blade loading) was about 0.5 at peak efficiency and design speed instead of the 0.33 value determined for the design conditions. For the overspeed tests, the rotor tip diffusion factor will increase above that at design speed and will be in a critical loading range (ref. 6). Consequently, it is possible that the decrease in peak efficiency at 106.4-percent design speed is due to high blade-element loadings.

Rotating-Stall and Surge Characteristics

The observations made with the hot-wire anemometers are presented to provide information about the rotating-stall characteristics of transonic-compressor rotors. Figure 9, a 60-percent-design-speed performance map, indicates the operating ranges at which the several different unsteady flow phenomena were observed. Changes in the stall characteristics are denoted on the performance map by letters for both decreasing weight flows (beneath curve) and increasing weight flows (above curve).

With decreasing weight flow, a rotor tip separation, as distinguished from normal blade wakes, was observed first at point A. At this condition, the separation seemed to affect only 1/4 inch of the span down from the rotor tip. Further decreases in weight flow caused the tip separation region to enlarge until the affected portion covered about 1/2 inch of the passage height at point B.

At the operating conditions between points B and C, three tip stall regions rotating in the direction of rotor rotation were observed. These stalls were of the partial-span type and affected about 35 percent of the passage height.

Between points C and D, a flow phenomenon was observed during which the pulsations picked up by two hot-wire anemometers were always in phase regardless of the relative circumferential or radial positions of the two probes. This phenomenon could not, therefore, be a periodic rotating stall, but must be an axial-flow pulsation or surge. The observed frequency was 46 cycles per second. At this condition, the pulsations were observed in the outer 70 percent of the annulus height. Pressure fluctuations of the same frequency as that noted with the hot-wire probes were also obtained in the inlet tank and collector by means of sensitive pressure pickups during the surge condition (C to D in fig. 9).

At point D of figure 9, a rotating-stall condition was again present. Two stall regions, covering the complete blade span and rotating in the direction of rotor rotation, existed from point D down to the lowest weight flow tested (point E). The flow fluctuations were smallest near the hub and greatest near the tip.

The following table summarizes the information obtained with the hot-wire anemometers at a corrected rotor rotational speed of 164 revolutions per second:

Location on performance map, fig. 9	Rotational speed of stall regions, rps	Number of stall regions	Ratio of stall rotational speed to rotor rotational speed	
			Absolute	Relative
B-C, G-H	134	3	0.816	0.184
D-E, E-F	104	2	.634	.366

The amplitude of the flow fluctuations observed during the tests of this rotor were of the same magnitude as those reported in reference 9.

SUMMARY OF RESULTS

The following preliminary results were obtained from an experimental investigation of a transonic axial-flow-compressor rotor designed and tested to obtain blade-element data on double-circular-arc airfoil sections. This rotor was designed for a total-pressure ratio of 1.34 with a design tip relative inlet Mach number of 1.10 at a corrected tip speed of 1000 feet per second and an inlet hub-tip ratio of 0.5.

1. Peak efficiency as determined from fixed-rake measurements at design speed was 0.89 at a corrected specific weight flow of 30.5 pounds per second per square foot of frontal area and an average total-pressure ratio of 1.41. Peak efficiency averaged about 0.92 for lower speeds down to and including 60 percent of design speed. The above-design total-pressure ratio resulted from an overturning of the air.

2. For this transonic rotor, a partial-span rotating stall, surge, and full-span rotating stall were observed as the weight flow was decreased.

Lewis Flight Propulsion Laboratory
National Advisory Committee for Aeronautics
Cleveland, Ohio, December 7, 1953

REFERENCES

1. Lieblein, Seymour, Lewis, George W., Jr., and Sandercock, Donald M.: Experimental Investigation of an Axial-Flow Compressor Inlet Stage Operating at Transonic Relative Inlet Mach Numbers. I - Over-All Performance of Stage with Transonic Rotor and Subsonic Stators up to Rotor Relative Inlet Mach Number of 1.1. NACA RM E52A24, 1952.

2. Robbins, William H., and Glaser, Frederick, W.: Investigation of an Axial-Flow Compressor Rotor with Circular-Arc Blades Operating up to a Rotor-Inlet Relative Mach Number of 1.22. NACA RM E53D24, 1953.

3. Schwenk, Francis C., Lieblein, Seymour, and Lewis, George W., Jr.: Experimental Investigation of Axial-Flow Compressor Inlet Stage Operating at Transonic Relative Inlet Mach Numbers. III - Blade-Row Performance of Stage with Transonic Rotor and Subsonic Stator at Corrected Tip Speeds of 800 and 1000 Feet Per Second. NACA RM E53G17, 1953.

4. Klapproth, John F.: General Considerations of Mach Number Effects on Compressor-Blade Design. NACA RM E53L23a, 1954.

5. Lieblein, Seymour: Review of High-Performance Axial-Flow-Compressor Blade-Element Theory. NACA RM E53L22, 1954.

6. Lieblein, Seymour, Schwenk, Francis C., and Broderick, Robert L.: Diffusion Factor for Estimating Losses and Limiting Blade Loadings in Axial-Flow-Compressor Blade Elements. NACA RM E53D01, 1953.

7. Carter, A. D. S.: The Low Speed Performance of Related Aerofoils in Cascade. Rep. No. R. 55, British N.G.T.E., Sept. 1949.

8. Lawrence, James C., and Landes, L. Gene: Auxiliary Equipment and Techniques for Adapting the Constant-Temperature Hot-Wire Anemometer to Specific Problems in Air-Flow Measurements. NACA TN 2843, 1952.

9. Huppert, Merle C.: Preliminary Investigation of Flow Fluctuations During Surge and Blade Row Stall in Axial-Flow Compressors. NACA RM E52E28, 1952.

TABLE I. - ROTOR BLADE-ELEMENT GEOMETRY

Radius, in.		Solidity, σ	Blade inlet angle, γ_3^o, deg		Blade outlet angle, γ_4^o, deg	
Inlet, r_3	Outlet, r_4		Design	Measured	Design	Measured
7.00	7.00	1.00	54.1	52.7	40.3	41.5
6.55	6.62	1.04	52.2	51.0	36.9	37.2
6.38	6.47	1.05	51.4	50.2	35.5	35.6
5.80	5.97	1.12	48.6	47.6	30.3	30.0
5.22	5.47	1.19	45.5	44.7	23.7	23.7
4.63	4.97	1.28	42.0	41.5	15.9	16.7
4.05	4.47	1.41	38.0	37.6	6.2	8.3

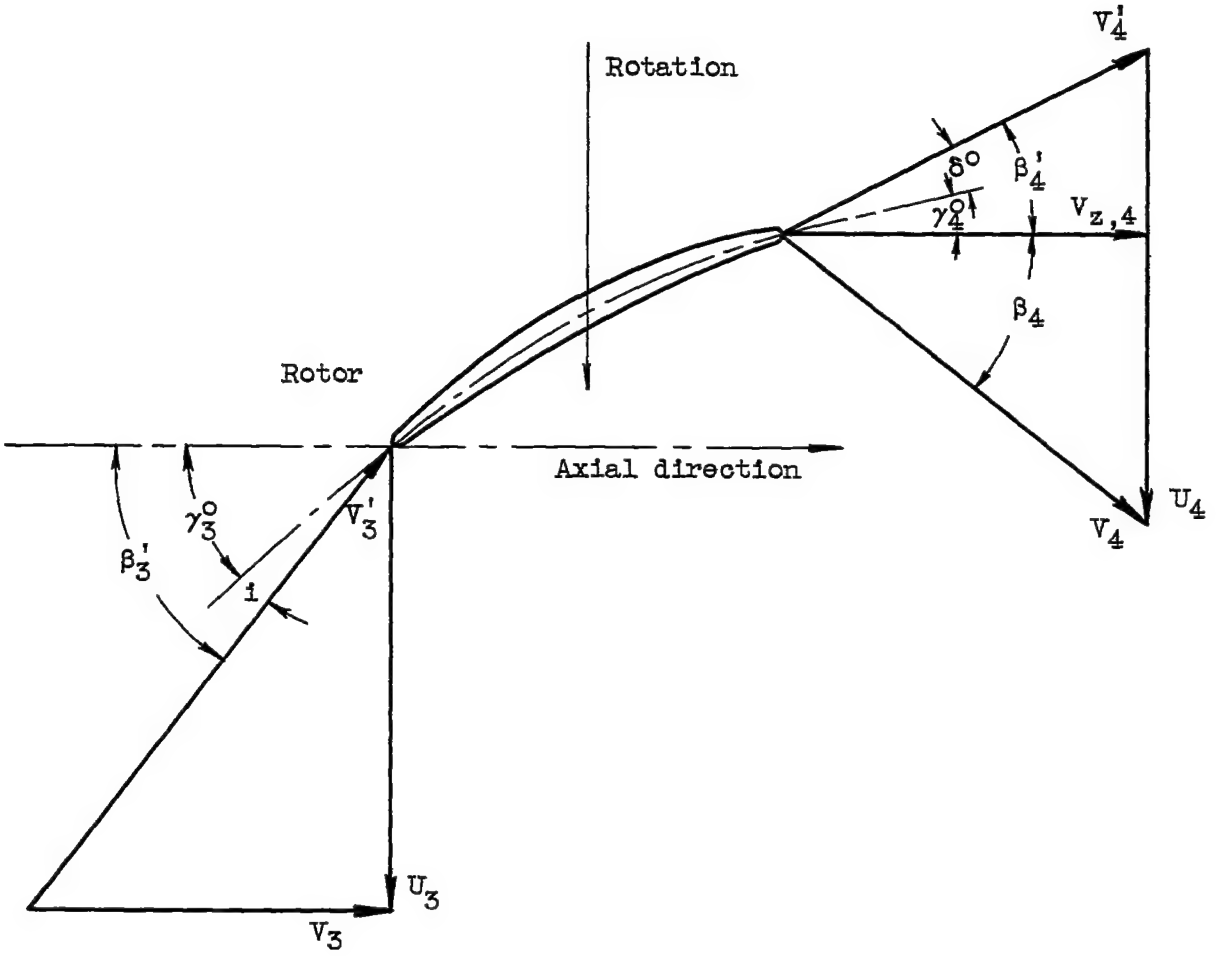

Figure 1. - Velocity-diagram notation for blade element.

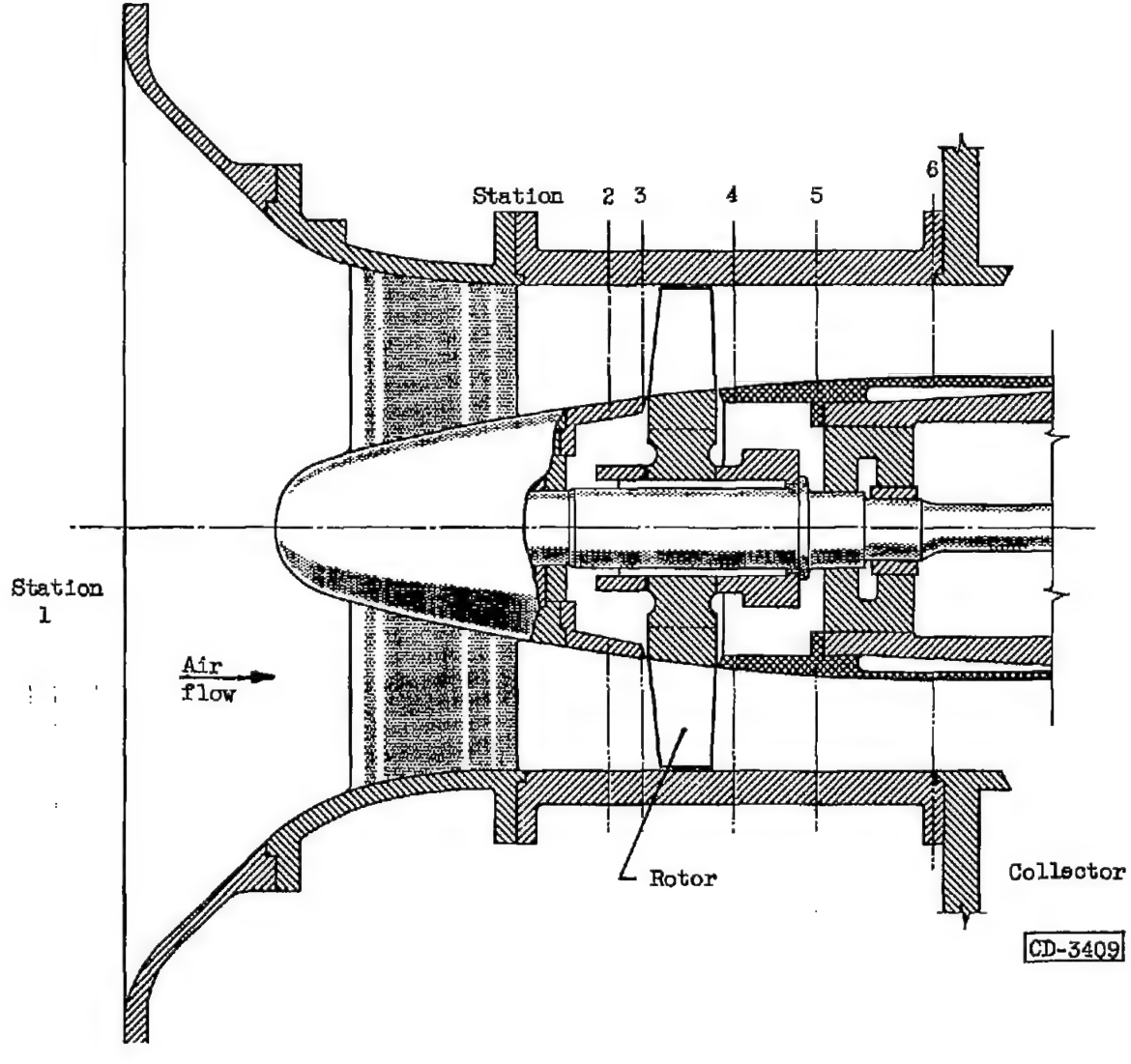

Figure 2. - Schematic diagram of 14-inch-tip-diameter variable-component transonic-compressor test rig.

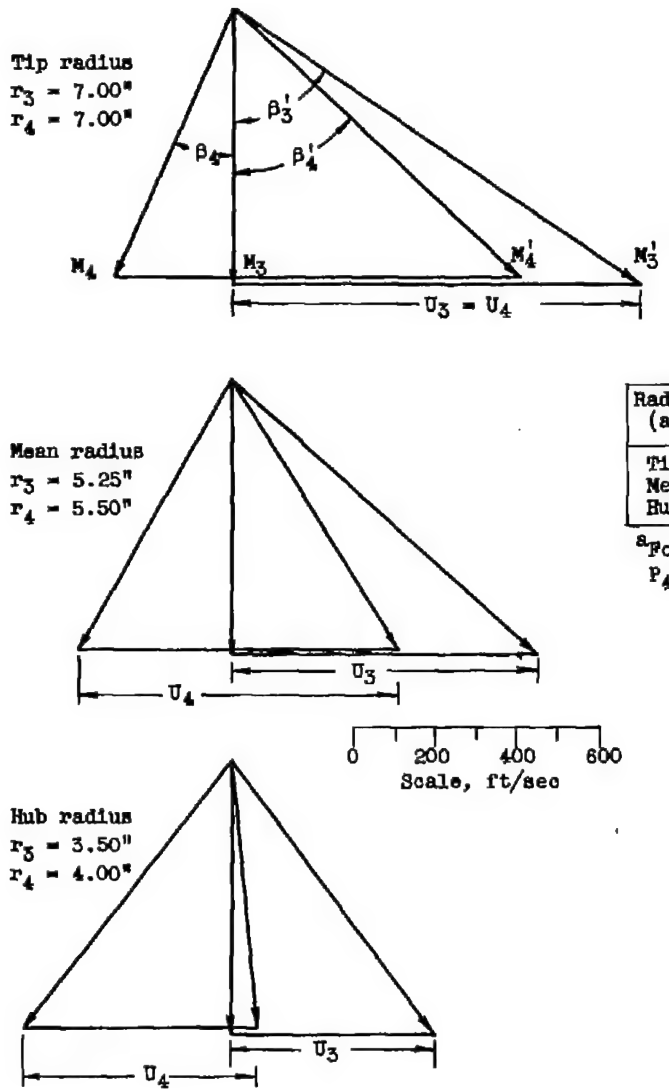

Radius (a)	M_3'	β_3', deg	M_4	β_4, deg	M_4'	β_4', deg	D
Tip	1.10	57.05	0.62	25.03	0.84	48.28	0.329
Mean	.92	49.30	.65	30.67	.67	33.40	.376
Hub	.76	37.70	.73	39.28	.57	5.19	.406

[a]For all three radii, M_3 = 0.80; β_3 = 0°; and P_4/P_3 = 1.34.

Figure 3. - Design vector diagrams at standard inlet conditions and design corrected tip speed of 1000 feet per second.

Figure 4. - Transonic rotor.

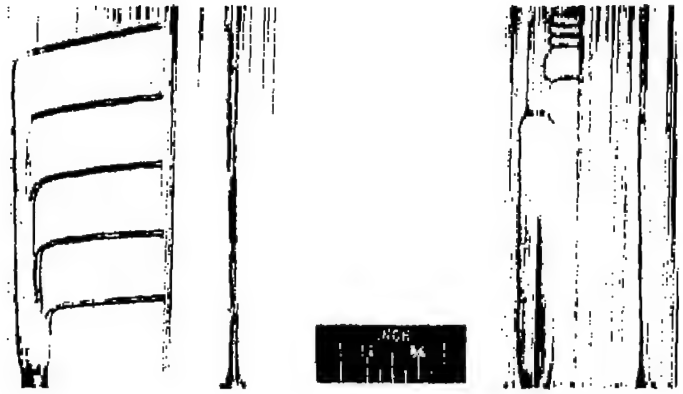

(a) Static-pressure rake. (b) Total-pressure rake.

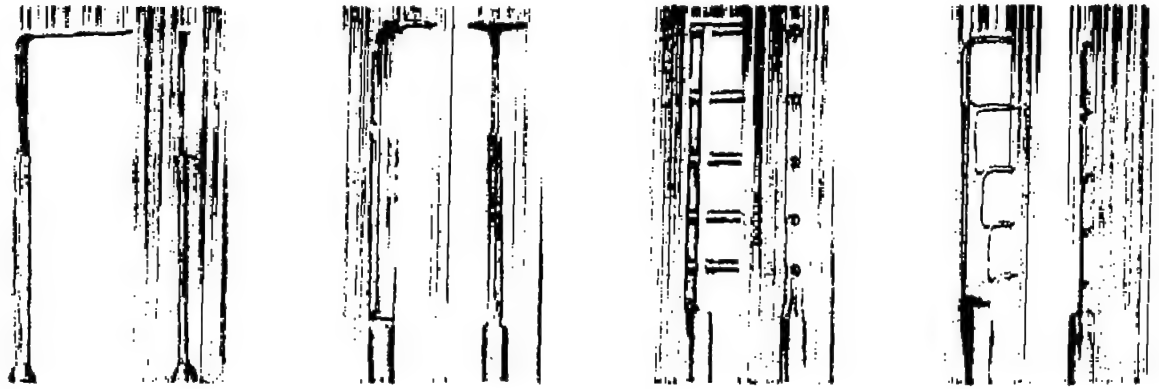

(c) L-head static-pressure probe. (d) Combination claw, total-pressure, total-temperature probe. (e) Shielded total-pressure rake. (f) Temperature rake.

C-34418

Figure 5. - Instrumentation used in tests of transonic-compressor rotor.

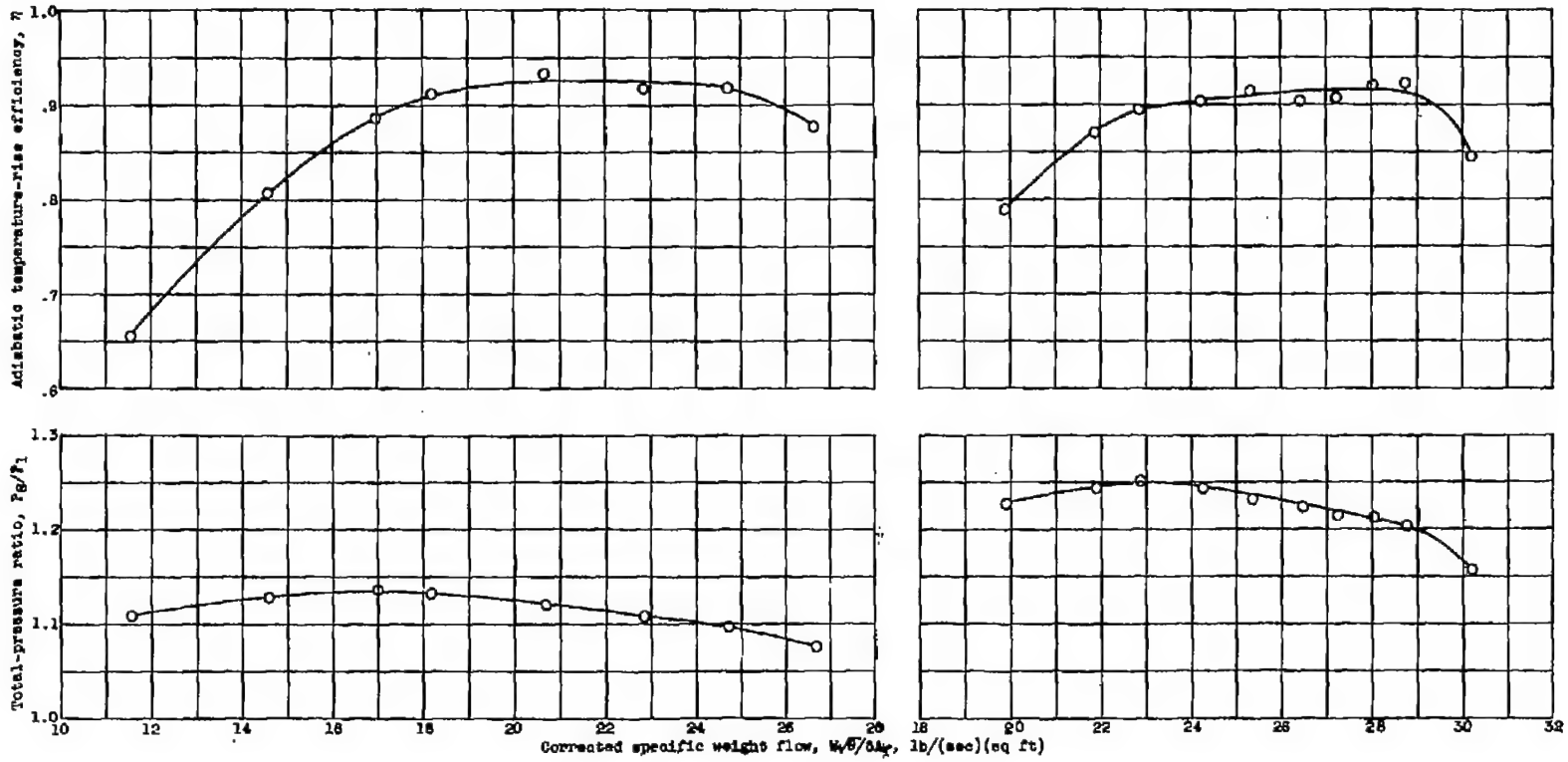

(a) Corrected tip speed, 600 feet per second.

(b) Corrected tip speed, 800 feet per second.

Figure 6. - Over-all performance of transonic rotor.

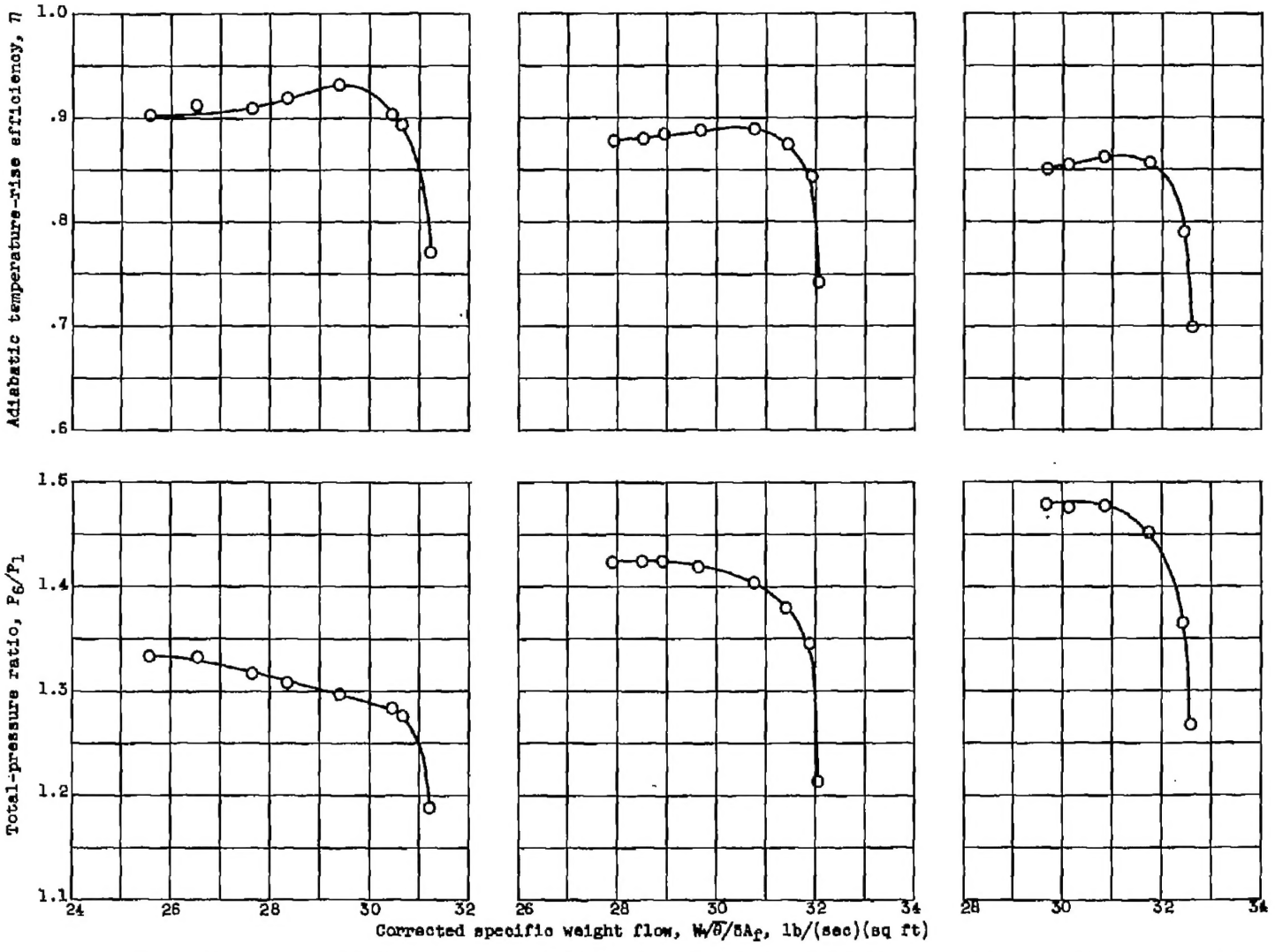

(c) Corrected tip speed, 900 feet per second.

(d) Corrected tip speed, 1000 feet per second.

(e) Corrected tip speed, 1064 feet per second.

Figure 6. - Concluded. Over-all performance of transonic rotor.

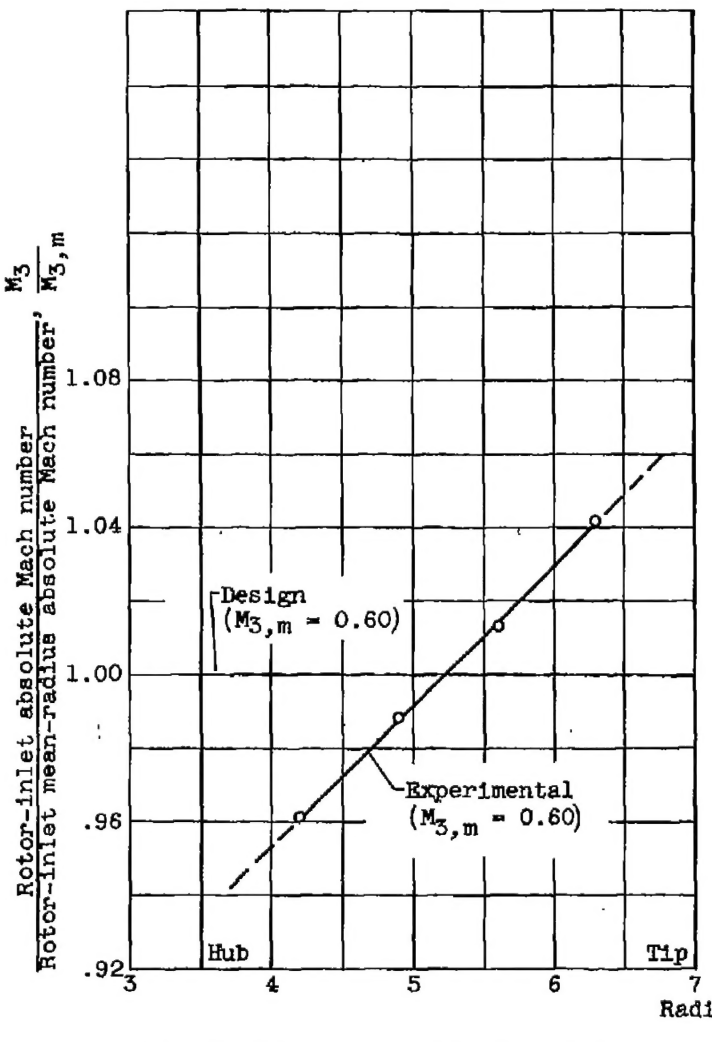

(a) Rotor-inlet absolute Mach number.

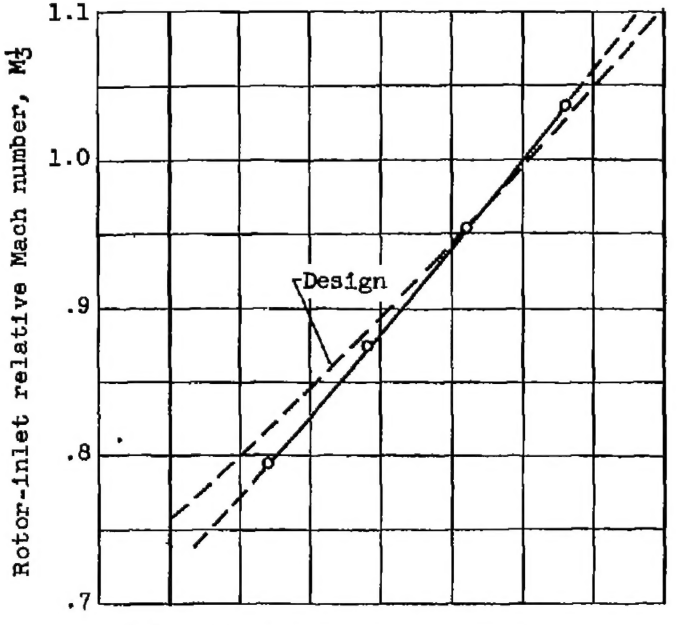

(b) Rotor-inlet relative Mach number.

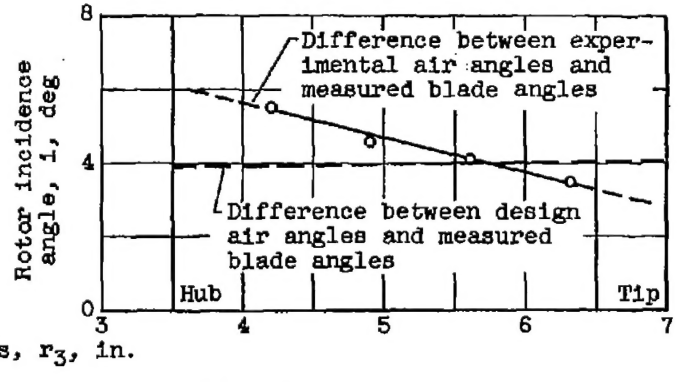

(c) Rotor incidence angle.

Figure 7. - Radial variation of rotor-inlet conditions at design corrected tip speed (1000 ft/sec) and corrected specific weight flow of 30.8 pounds per second per square foot of frontal area.

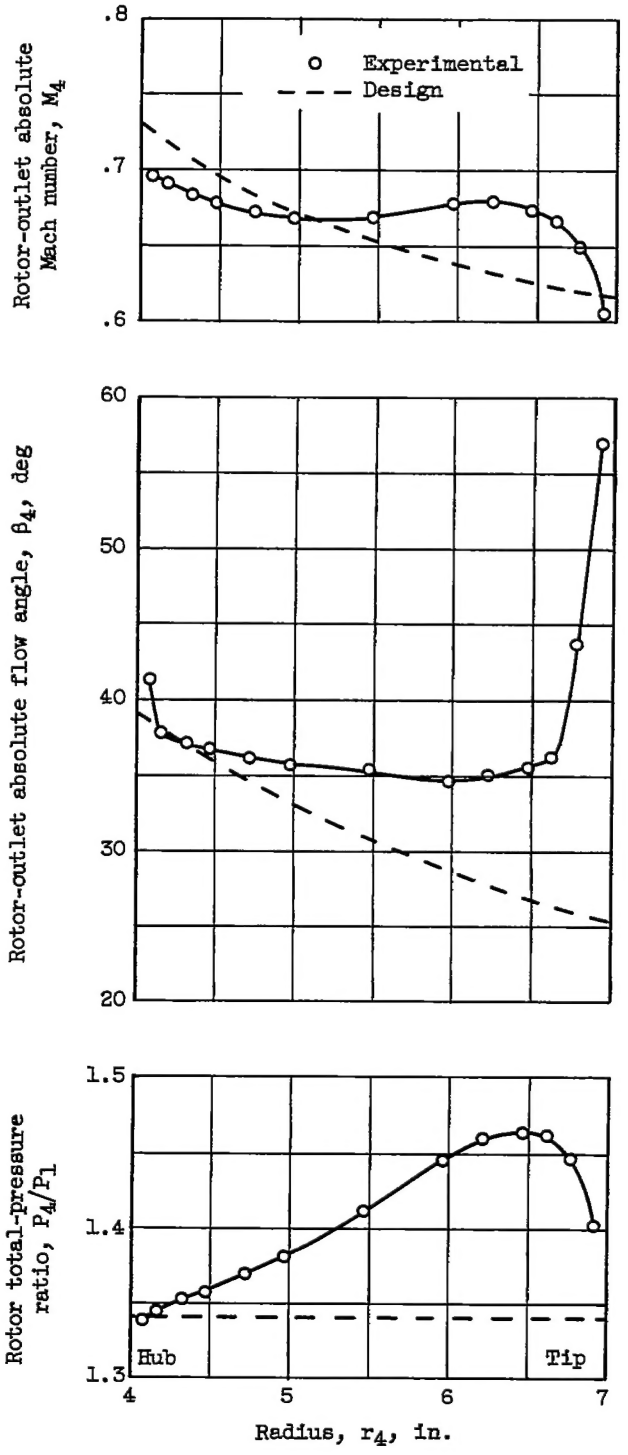

Figure 8. - Radial variation of rotor-outlet flow properties at design corrected tip speed (1000 ft/sec) and a corrected specific weight flow of 30.8 pounds per second per square foot of frontal area.

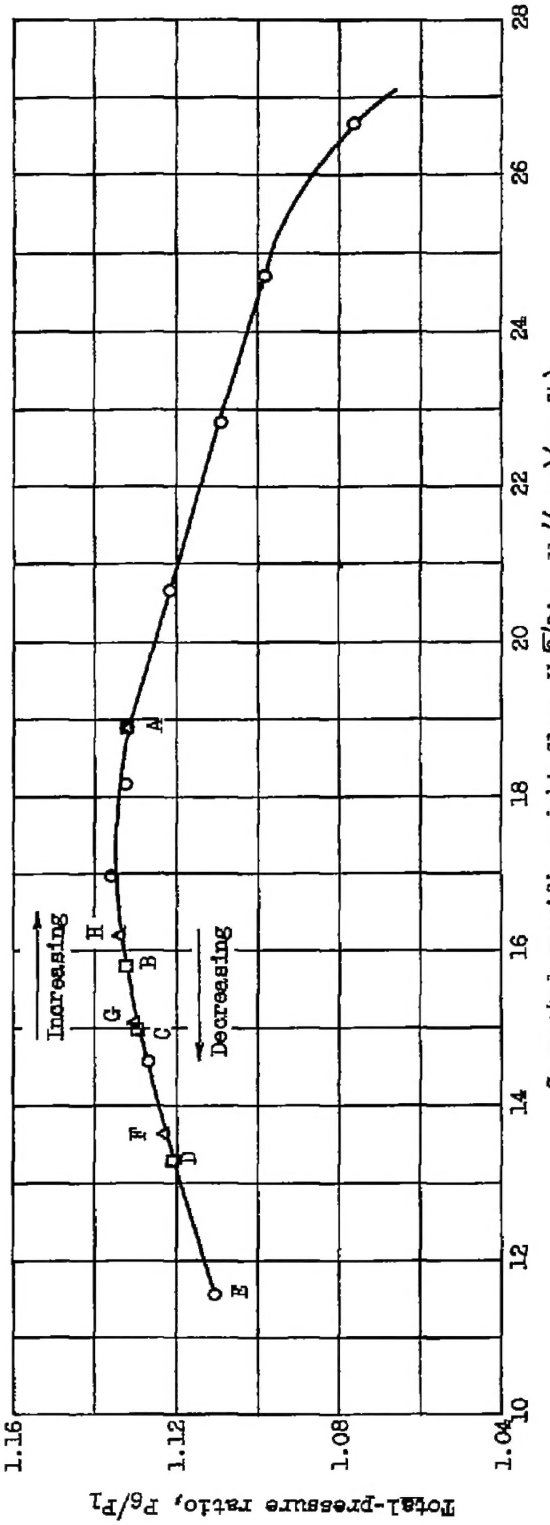

Figure 9. - Over-all performance of transonic-compressor rotor at 60-percent design speed, indicating stall and surge regions. Corrected rotor rotational speed, 164 rps.

NACA-Langley - 4-8-54 - 325